Influence of Initial Conditions on the WRF–ARW Model QPF Response to Physical Parameterization Changes

Isidora Jankov* and William A. Gallus Jr.

Department of Geological and Atmospheric Science, Iowa State University, Ames, Iowa

Moti Segal

Department of Agronomy, Iowa State University, Ames, Iowa

Steven E. Koch

NOAA/ESRL/Global Systems Division, Boulder, Colorado

ABSTRACT

To assist in optimizing a mixed-physics ensemble for warm season mesoscale convective system rainfall forecasting, the impact of various physical schemes as well as their interactions on rainfall when different initializations were used has been investigated. For this purpose, high-resolution Weather Research and Forecasting (WRF) model simulations of eight International H_2O Project events were performed. For each case, three different treatments of convection, three different microphysical schemes, and two different planetary boundary layer (PBL) schemes were used. All cases were initialized with both Local Analyses and Prediction System (LAPS) "hot" start analyses and 40-km Eta Model analyses. To evaluate the impacts of the variation of two different physical schemes and their interaction on the simulated rainfall under the two different initial conditions, the factor separation method was used. The sensitivity to the use of various physical schemes and their interactions was found to be dependent on the initialization dataset. Runs initialized with Eta analyses appeared to be influenced by the use of the Betts–Miller–Janjić scheme in that model's assimilation system, which tended to reduce the WRF's sensitivity to changes in the microphysical scheme compared with that present when LAPS analyses were used for initialization. In addition, differences in initialized thermodynamics resulted in changes in sensitivity to PBL and convective schemes. With both initialization datasets, the greatest sensitivity to the simulated rain rate was due to changes in the convective scheme. However, for rain volume, substantial sensitivity was present due to changes in both the physical parameterizations and the initial datasets.

1. Introduction

To assist in optimizing a mixed-physics ensemble for warm season continental mesoscale convective system (MCS) rainfall forecasting, Jankov et al. (2005) evaluated the impact that various physical schemes as well as their interactions had on rainfall forecast skill in high-resolution [12-km grid spacing with the Advanced Research Weather and Research Forecasting (WRF) model (ARW) dynamic core; 34 vertical levels] simulations of eight International H_2O Project (IHOP) events. A general description of IHOP is given in Weckwerth and Parsons (2006). All runs were initialized with a diabatic Local Analyses and Prediction System (LAPS) "hot" start initialization (Jian et al. 2003). Jankov et al. (2005) found that no single model configuration was clearly better than the rest. In terms of skill measures, the best configuration varied both with the prediction time and rainfall threshold. In addition, the results implied that if an ensemble designed for MCS rainfall prediction lacks sufficient spread, model

_____

* Current affiliation: Cooperative Institute for Research in the Atmosphere, Colorado State University, Fort Collins, Colorado.

_____

Corresponding author address: Isidora Jankov, NOAA/ESRL, GSD7, 325 Broadway, Boulder, CO 80305-3328.
E-mail: isidora.jankov@noaa.gov

runs with different convective schemes should be included as the most efficient way to increase the spread substantially. On the other hand, for hydrological purposes when rain volume is a desired quantity, model runs with Ferrier et al. (2002) and Lin et al. (1983) microphysical schemes may require different bias corrections or weightings in an ensemble compared with runs using National Centers for Environmental Prediction-5 (NCEP-5) class microphysics (Hong et al. 1998).

The present study further addresses issues raised in Jankov et al. (2005). It adopts the same approach with the same matrix of 18 different model configurations but compares the sensitivity to the parameterizations in runs using 40-km NCEP Eta Model gridded binary (GRIB) data as initial and boundary conditions to the sensitivity in runs using a LAPS hot start for initialization. The main focus of the present study is to investigate if and how the impact of the physical schemes and their interaction changes when different initial conditions are used. Such an evaluation has two merits: (i) further exploring the WRF–ARW model's prediction performance and (ii) providing an additional insight relevant to the ensemble prediction of convection under varied physical schemes and initial conditions. To perform this evaluation, some of the results from Jankov et al. (2005) will be used in the present study. Methodologies used in this paper are described in section 2, results in section 3, with a concluding summary and discussion in section 4.

2. Methodology

As in Jankov et al. (2005), the WRF–ARW model, version 1.3, was used for simulations of eight 2002 IHOP convective cases (initialized at 0600 UTC 16 May, 1200 UTC 23 May, 1800 UTC 24 May, 1200 UTC 2 June, 0000 UTC 4 June, 0000 UTC 13 June, 0600 UTC 15 June, and 1200 UTC 19 June) with 18 different combinations of physical schemes. The integration domain covered a roughly 1500 km $\times$ 1500 km region centered over the south-central United States (see Fig. 5 for a map of the domain). For each case, three different treatments of convection were used: the Kain–Fritsch (KF) scheme (Kain and Fritsch 1993; Kain 2004), the Betts–Miller–Janjić (BMJ) scheme (Betts 1986; Betts and Miller 1986; Janjić 1994), and the use of a nonconvective scheme. For an elaboration on performance differences between the KF and BMJ schemes, see Jankov and Gallus (2004). For each of these three convection treatments, three different microphysical schemes were used: Lin et al. (1983), NCEP-5 class (Hong et al. 1998),

TABLE 1. Notation used for different physical schemes and initializations in the present study. Physical schemes used in the control run are marked with an asterisk.

Physical scheme/initialization	Notation
Physical scheme	
Betts–Miller–Janjić convection	BMJ
Kain–Fritsch convection*	KF
Run without convection	NC
Eta PBL	ETA
MRF PBL*	MRF
Lin et al. microphysics	MPL
NCEP-5 microphysics*	MPN
Ferrier microphysics	MPF
Initialization	
40-km NCEP Eta	Eta
LAPS hot start	LAPS

and Ferrier et al. (2002). Within these nine possible configurations, two different PBL schemes were used: the Medium-Range Forecast (MRF) (Troen and Mahrt 1986; Hong and Pan 1996) and the Eta (often referred to as Mellor–Yamada–Janjić model, version 2.5; Janjić 2001) schemes. For all model runs the same longwave radiative scheme (Rapid Radiative Transfer Model; Mlawer et al. 1997), shortwave radiative scheme (Dudhia 1989), and land surface model scheme (Chen and Dudhia 2001) were used. The "control run," as in Jankov et al. (2005), was chosen to match the real-time model configuration adopted by the National Oceanic and Atmospheric Administration's (NOAA's) Forecast Systems Laboratory during the IHOP experiment. It used the KF convective scheme, the MRF PBL scheme, and the NCEP-5 class microphysical scheme. The abbreviations used in this study for runs with different combinations of physical schemes and the initialization datasets are found in Table 1. A total of 288 WRF–ARW simulations were considered in the present study (see appendix A for a statement related to simulations that used the MPF scheme). For rainfall validation, observed 6-h accumulated rainfall from the NCEP stage IV analysis (Baldwin and Mitchell 1997) was used.

In the present study all runs were initialized with 40-km NCEP Eta Model GRIB data, and integrated for 24 h. Comparisons are made with the Jankov et al. (2005) results, which used the diabatic LAPS hot-start initialization (Jian et al. 2003). The LAPS hot-start technique is based on a three-dimensional analysis of cloud attributes using radar, satellite, and surface data, combined with a method of estimating hydrometeor mixing ratios, precipitable water, and cloud vertical motions. By using a variational adjustment procedure (involving dynamic balancing and a mass conservation

constraint), horizontal wind fields and the mass field are adjusted to produce divergence consistent with the assumed cloud updraft properties (depth, magnitude, and shape of the updraft profiles). Essentially, LAPS analyses include the initialization of hydrometeors, while that is not the case for the Eta Data Assimilation System (EDAS). This should result in an immediate activation of microphysical schemes and simulation of the grid-resolved precipitation component at early forecast times in the case of runs initialized with LAPS analyses. On the other hand, for runs initialized with Eta analyses the model dynamics start off with an unsaturated initial state and, therefore, a delay in the activation of the microphysics should be expected.

Also, it should be pointed out that the hot-start approach was developed for grid spacings that resolve saturated updrafts and compensating subsidence, but it is still used quasi-operationally for much coarser resolutions ($\Delta x > 10$ km). Coarser resolution requires the use of a convective parameterization, which may lead to a mismatch between the hot-start grid-resolved vertical motion and grid-scale vertical motions associated with a cumulus parameterization scheme. Nonetheless, the emphasis of the hot start is to initiate the forecast with a vertical motion field that is at least qualitatively consistent with the initial hydrometeor field. It is presumed that this vertical motion mismatch is not the cause of serious problems. As a measure of forecast accuracy, an equitable threat score (ETS; Schaefer 1990) and bias were calculated. A quantification of an impact of varying two different model physical schemes on the simulated rainfall field was performed by using the factor separation methodology formulated by Stein and Alpert (1993). Based on this methodology,

$$f_{xy} - f_0 = (f_x - f_0) + (f_y - f_0) + \hat{f}_{xy}, \qquad (1)$$

where f_0 represents the control run simulated rainfall amount, f_{xy} represents the rainfall amount simulated by a run with changes in both physical schemes of interest (two physical schemes changed compared to the control run), f_x represents the rainfall amount produced by a run that has one of the two physical schemes of interest changed (as compared to the control run), f_y represents the rainfall amounts simulated by a run with another physical scheme of interest changed (as compared to the control run), and $\hat{f}_{xy}$ stands for a synergistic term [$\hat{f}_{xy} = f_{xy} - (f_x + f_y) + f_0$] reflecting the rainfall amount contributed by the nonlinear interaction between the two physical

schemes. This term may be thought of as the difference between the actual rainfall occurring in the run in which two schemes have been changed and the rainfall expected by adding the impacts of each individual change. When the synergistic term is equal to zero, no rainfall is attributed to the interaction of the two changed physical schemes.

The factor separation method was applied for an analysis of two different rainfall measures: system-average rain rate (rain depth integrated for amounts exceeding a specified threshold averaged over the area where the threshold was exceeded; hereafter, rain rate), and domain-total rain volume (rain depth integrated for amounts exceeding a specified threshold, averaged over the whole simulated domain; hereafter, rain volume). The use of both measures characterizes the QPF better, because two runs could have the same total rain volume with one achieving it through light rainfall over a large area and the other through heavy rainfall in a small area. As part of the evaluation of changes in rain rate and rain volume due to variations in physical schemes, statistical significance testing was performed. For the rigorous hypothesis testing, Hamill's (1999) resampling methodology was used. The null hypotheses for the resampling tests were that differences in rain rates, rain volumes, ETSs, or biases between the two opposing forecasts were equal to zero. Based on the null hypotheses, the test statistics and resampled distributions were formed. The resampled statistics were formed by randomly choosing either one or the other forecast and then calculating differences between them (i.e., rain rate, rain volume, or contingency table elements in the case of ETS and bias calculations). This procedure was repeated 1000 times for both a separate treatment of each 6-hourly forecast period and for all 6-h periods combined. Combining all forecast periods together helped to increase the small sample size to better evaluate the statistical significance. This technique to enlarge the sample size was only valid when statistical stationarity was present and was not appropriate for cases in which variables were characterized by strong temporal variability. Also, to investigate if the statistical significance testing by combining all four 6-h forecasts together was impacted by the spinup usually associated with runs initialized with Eta analyses during the first six forecast hours, the statistical significance testing was performed with both first 6-h forecasts from runs initialized with Eta analyses included and excluded. The same trends were obtained. Finally, the hypotheses of the differences in rain rate, rain volume, ETS, or bias were tested by determining the location of the difference within the resampled distribution, or

in other words, by calculating the corresponding *p* value.

In the present study, the discussion will be focused on the statistically significant results. The notation presented in Table 1 will be used to indicate different model configurations. The control configuration is labeled with an asterisk in Table 1 (KF–MRF–MPN).

3. Results

a. Sensitivity of rainfall forecast skill to physical scheme changes under different initial conditions

ETSs and bias values averaged for all eight cases for all 18 model configurations indicated that no one configuration was obviously best at all times for all thresholds with both initializations (see appendix B for more details). Figure 1 illustrates the ETS and bias averaged for the six configurations of the KF, BMJ, and NC runs for both initializations, during the 0–6-h forecast period. It can be seen that for lighter thresholds the highest ETSs (Fig. 1a), accompanied by a slight positive bias error (Fig. 1b), were associated with NC runs initialized with LAPS analyses. These high ETSs might be explained by the impact of the hot-start initialization. This initialization incorporates the ongoing precipitation in the model, as discussed in section 2. In this way the spinup effect and precipitation delay that are often associated with runs without convective parameterizations are minimized. For runs using convective schemes, errors related to the schemes are still present resulting in a lower skill compared with NC runs. For the heavier thresholds, NC runs tended to have the lowest ETSs. A subjective analysis showed that the low ETS values associated with NC runs were very frequently related to a displacement error. The low ETSs are also consistent with the fact that the NC runs always had lower bias values compared to runs using convective schemes.

For runs initialized with Eta analyses, the highest ETSs for lighter and moderate thresholds were found for the BMJ runs (Fig. 1c). These high ETSs might be related to the fact that the EDAS uses the BMJ scheme. Thus, initialized thermodynamics (which are tuned for the BMJ scheme) may favor the activation of the BMJ scheme during the early forecast hours. In addition, the BMJ scheme has a tendency to generate large areas of light rainfall (Jankov and Gallus 2004), yielding a high bias (Fig. 1d), which is usually associated with higher ETSs (Mason 1989).

Later in time, during the 12–18-h forecast period (Fig. 2), for lighter thresholds, the highest ETSs were
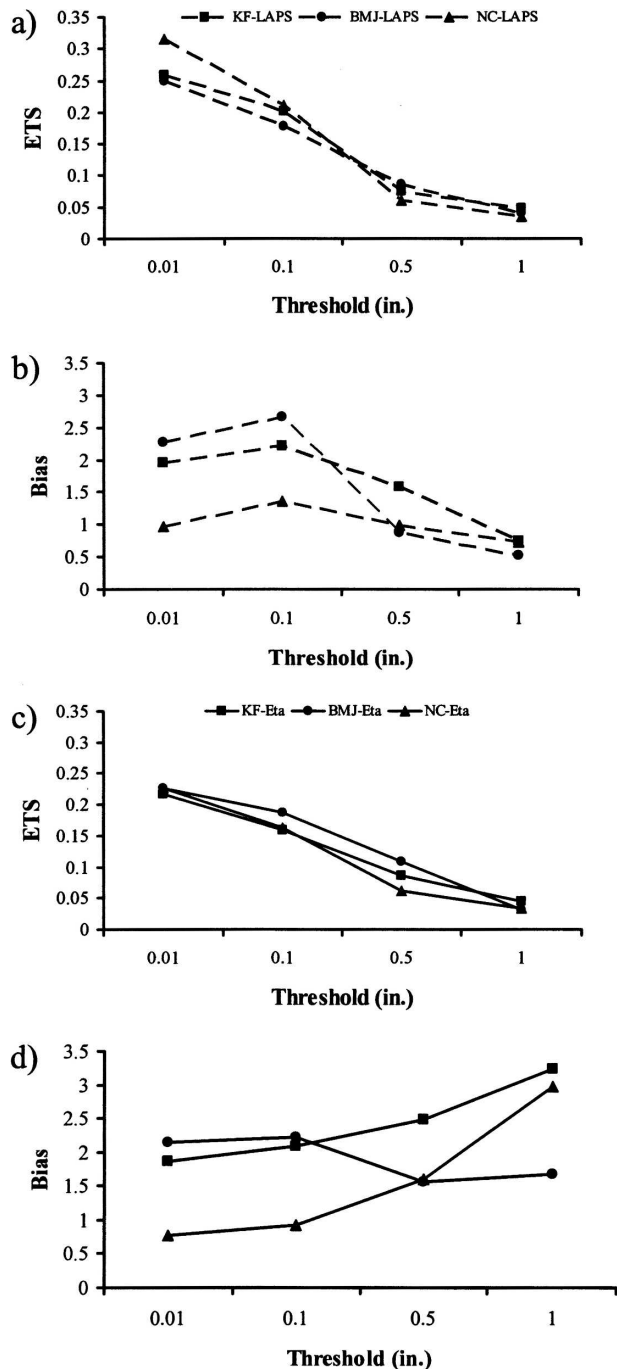

FIG. 1. Average (a) ETS and (b) bias for the 0–6-h forecast period for the six configurations associated with the KF, BMJ, and NC runs initialized with the LAPS initialization. (c), (d) As in (a) and (b), respectively, but for the Eta initialization.

generally associated with NC runs initialized with LAPS analyses and with BMJ runs initialized with Eta analyses. In the case of NC runs, bias values were about 1 while in the case of BMJ runs they
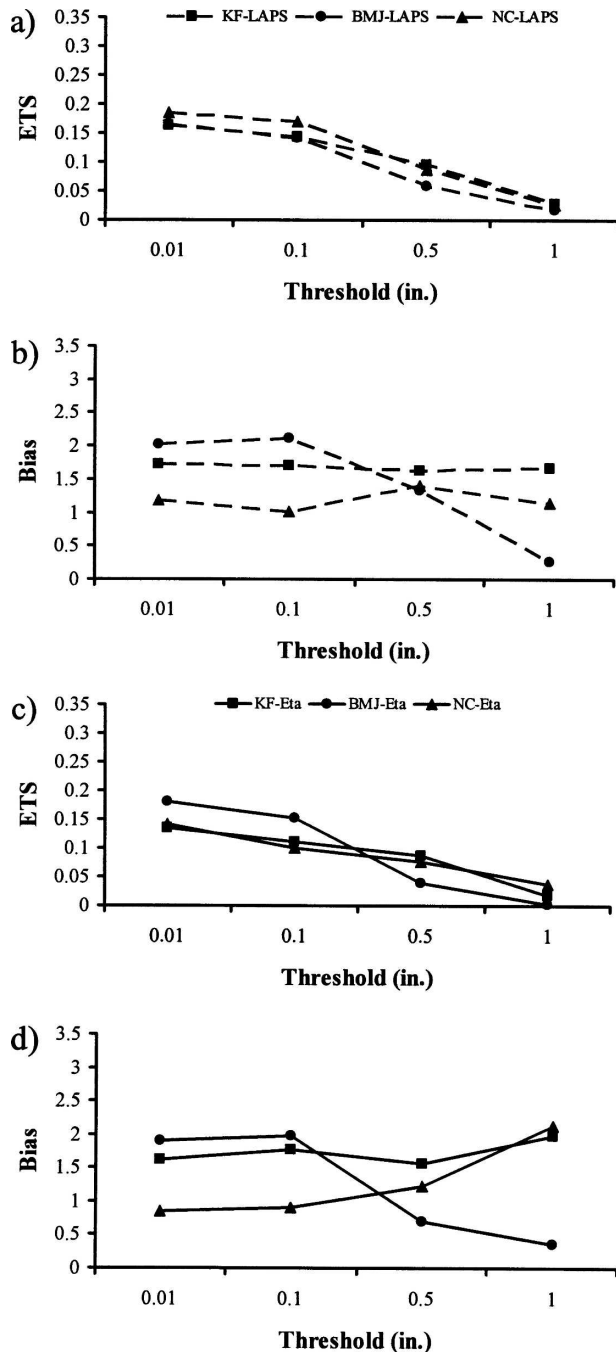
a)

b)

c)

d)

FIG. 2. As in Fig. 1 but for the 12–18-h forecast period.

were higher, and around 2. For heavier thresholds NC runs had the highest ETSs and biases associated with them had increased compared to earlier times and were now comparable to runs using the KF convective scheme.

Figures 3 and 4 illustrate differences in ETS and bias for (i) runs when the initial conditions were changed

and the model configuration was kept the same and (ii) runs initialized with the two initial conditions when the model control configuration was also changed (i.e., KF changed to BMJ or NC, MRF changed to ETA, and MPN changed to either MPL or MPF), for two different thresholds (0.01 and 0.5 in.), during the 0–6- and 12–18-h forecast periods. Thus, for example, the notation IC-BMJ indicates differences between ETSs and biases averaged for the six model configurations using the BMJ scheme for the two different initial conditions, while PP-BMJ indicates the differences in ETSs and biases between the averages of the six model configurations using the BMJ scheme and the model control configuration and then averaged for both initial conditions. It can be seen that differences in ETS (Figs. 3a and 4a) were more influenced by changes in initial conditions, especially for the 0.01-in. threshold during the 0–6-h forecast period. On the other hand, bias differences (Figs. 3b and 4b) due to changes in initial conditions and changes in the model configuration were generally comparable for both thresholds and for both forecast periods.

For the 0.01-in. threshold during the early forecast period, runs initialized with LAPS analyses had higher ETSs (usually statistically significant) compared with runs initialized with Eta analyses (Fig. 3a). These higher ETSs were associated with higher biases (Fig. 3b). For the 0.5-in. threshold, runs initialized with LAPS analyses were generally characterized with lower ETSs and much smaller biases. The only exceptions were runs using ETA and MPL that had slightly higher ETSs but opposite trends in bias. The MPL runs initialized with LAPS analyses were characterized by small bias, while the opposite was the case for the ETA runs.

For the 0–6-h forecast period with the 0.01-in. threshold, a statistically significant impact on ETS occurred only for a change from KF to NC (Fig. 3a). With regard to changes in bias, they were generally larger with different physics configurations than with different initial conditions. For the heavier threshold the largest impacts on ETS were associated with changes from KF to both BMJ and NC.

During the 12–18-h forecast period, nearly all runs initialized with LAPS analyses were characterized by higher ETSs and biases compared with runs initialized with Eta analyses (Fig. 4). Statistically significant changes in ETS values due to a change in the initial conditions occurred at the 0.01-in. threshold for runs using NC and MPL, and at the 0.5-in. threshold for the BMJ and MPL runs.

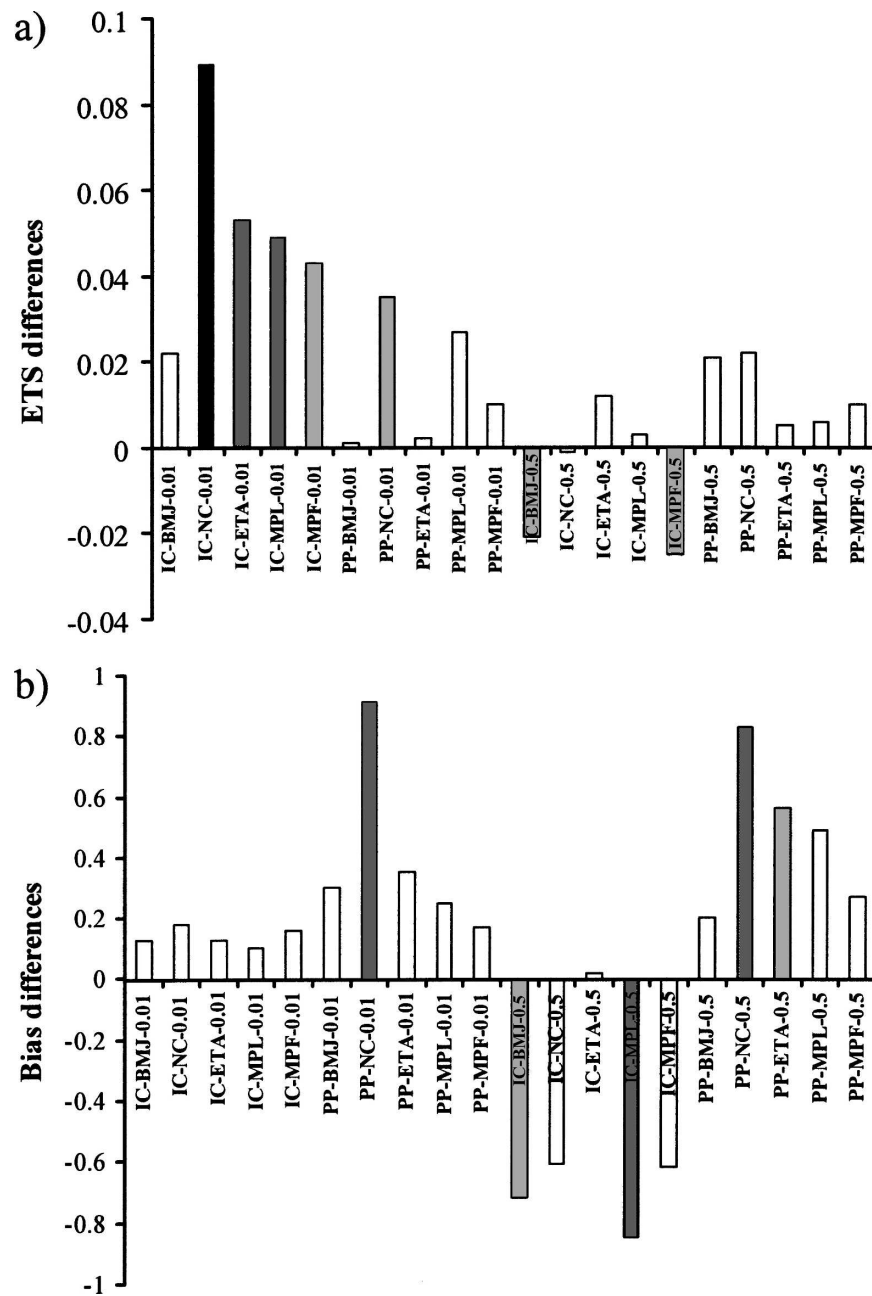With regard to ETS changes due to varying model

FIG. 3. Differences in (a) ETS and (b) bias when the initial conditions were changed (LAPS runs − ETA runs) while the physical parameterizations are kept the same (IC), and when the physical parameterizations were changed (PP), and differences in skill scores averaged for the two different initial conditions, for the 0.01- and 0.5-in. thresholds, during the 0–6-h forecast period. Bars shaded in black, dark gray, and gray indicate results that are statistically significant at the 95%, 90%, and 80% confidence levels, respectively.

configurations, statistically significant impacts only occurred for BMJ runs at the 0.01-in. threshold. Changes in bias were comparable to those associated with changes in the initial conditions for both thresholds. The overall comparable magnitudes of the changes in

ETS and bias from the changes in the physics and initial conditions imply that the ensemble spread might be effectively increased by the use of variations in both the initial conditions and physical schemes (Stensrud et al. 2000; Grimit and Mass 2002).
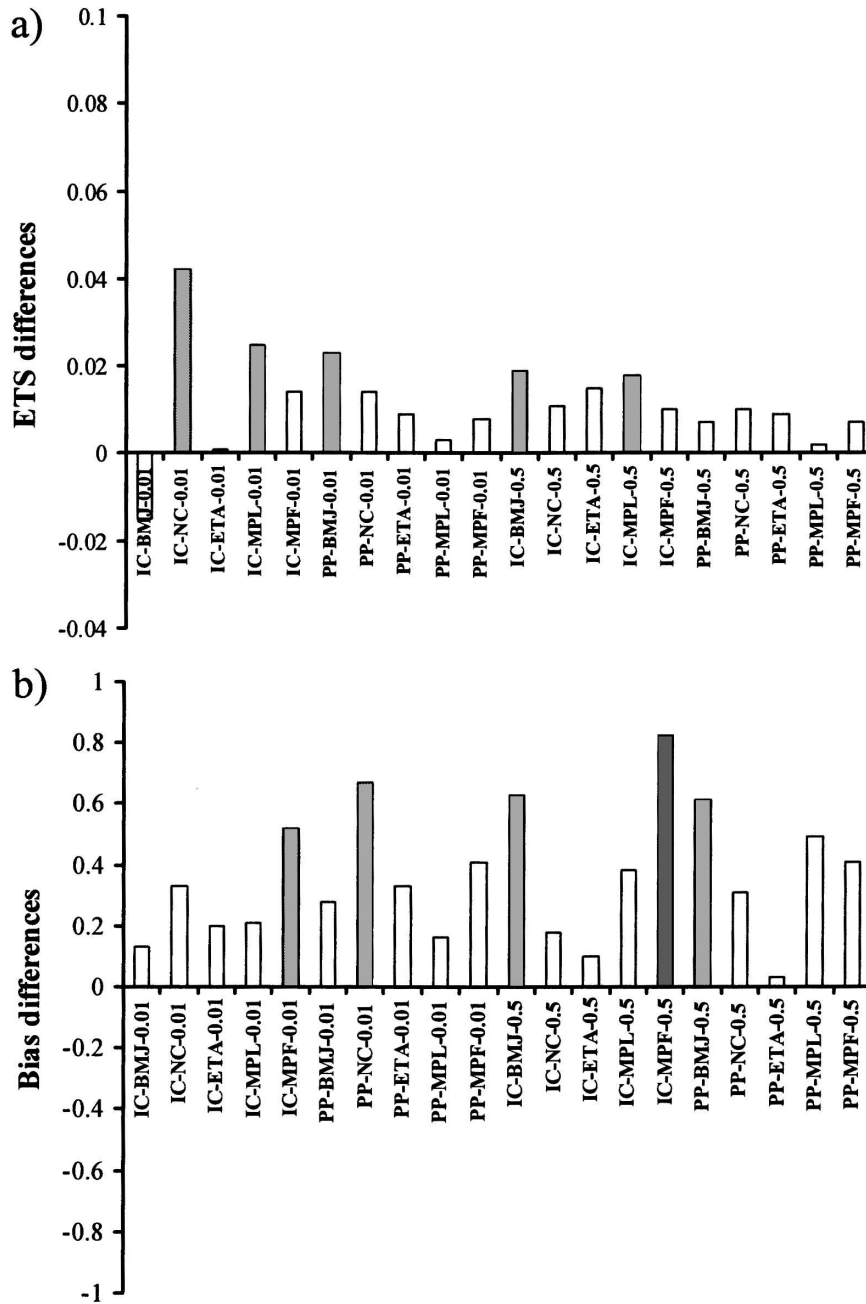
FIG. 4. As in Fig. 3 but for the 12–18-h forecast period.

b. Sensitivity of system-average rain rate and domain-total rain volume to physical scheme changes under different initial conditions

1) QUANTITATIVE RESULTS

The factor separation methodology was used to evaluate the sensitivity of both the rain rate (Table 2) and the rain volume (Table 3) to changes in the physical schemes when two different initializations were used.

The tables show the changes in rainfall due to individual changes in the physical schemes, as expressed by $(f_x - f_0)$ or $(f_y - f_0)$, and due to synergistic interactions between the two physical schemes, as expressed by $\hat{f}_{xy}$ [see Eq. (1)].

Only results that are statistically significant are presented. Table 2 shows the impact on rain rate for runs initialized with both LAPS and Eta analyses for two different thresholds (0.01 and 0.5 in.). It was found that

TABLE 2. Time series of percentage changes in system rain rate (see section 2 for the definition of system rain rate) averaged for all eight cases, due to physics changes (f_1 represents rainfall from the KF–ETA–MPN run, f_2 represents rainfall from KF–MRF–MPL, f_3 represents rainfall from KF–MRF–MPF, f_4 represents rainfall from NC–MRF–MPN, and f_5 represents rainfall from BMJ–MRF–MPN) averaged over points where rainfall exceeded specified thresholds (0.01 and 0.5 in.) for two different initializations (LAPS and Eta). Here, f_0 represents rainfall in the control run (KF–MRF–MPN), and $\hat{f}_{13}$, $\hat{f}_{24}$, and $\hat{f}_{34}$ represent corresponding synergistic terms. Values presented in boldface–italics, boldface, and italics indicate results that are statistically significant at the 95%, 90%, and 80% confidence levels, respectively.

Threshold (in.)	Initialization	Forecast period (h)			
		0–6	6–12	12–18	18–24
	LAPS analysis				
0.01	$(f_2 - f_0)/f_0$ (%)	5	*16*	*16*	*39*
	$(f_3 - f_0)/f_0$ (%)	**10**	**14**	*12*	**22**
	$(f_4 - f_0)/f_0$ (%)	***52***	***55***	***37***	***10***
0.5	$(f_2 - f_0)/f_0$ (%)	2	0	8	*25*
	Eta analysis				
0.01	$(f_2 - f_0)/f_0$ (%)	**9**	5	6	*26*
	$(f_3 - f_0)/f_0$ (%)	6	1	7	5
	$(f_4 - f_0)/f_0$ (%)	***31***	***24***	4	**21**
	$(f_5 - f_0)/f_0$ (%)	***−29***	***−45***	***−47***	***−48***
	$\hat{f}_{24}/f_0$ (%)	***28***	***100***	***85***	***80***
	$\hat{f}_{34}/f_0$ (%)	*−19*	−9	−12	*−32*
0.5	$(f_1 - f_0)/f_0$ (%)	**2**	**4**	**8**	**15**
	$(f_2 - f_0)/f_0$ (%)	***16***	**8**	2	**21**
	$(f_5 - f_0)/f_0$ (%)	***−15***	***−25***	***−44***	**−20**
	$\hat{f}_{13}/f_0$ (%)	−1	−3	−1	*−17*
	$\hat{f}_{24}/f_0$ (%)	*1*	***37***	***41***	**23**

TABLE 3. As in Table 2 but for domain-total rain volume (see section 2 for the definition of domain-total rain volume).

Threshold (in.)	Initialization	Forecast period (h)			
		0–6	6–12	12–18	18–24
	LAPS analysis				
0.01	$(f_2 - f_0)/f_0$ (%)	***37***	***32***	***53***	***94***
	$(f_3 - f_0)/f_0$ (%)	***26***	***22***	***22***	***46***
0.5	$(f_2 - f_0)/f_0$ (%)	***59***	***72***	***94***	***180***
	$(f_3 - f_0)/f_0$ (%)	***37***	***54***	***41***	***101***
	$(f_5 - f_0)/f_0$ (%)	***−50***	***−68***	***−69***	***−91***
	$\hat{f}_{12}/f_0$ (%)	*0*	***−25***	**−20**	***−83***
	$\hat{f}_{13}/f_0$ (%)	**14**	*−15*	***−39***	***−27***
	Eta analysis				
0.01	$(f_1 - f_0)/f_0$ (%)	**8**	**7**	***13***	***22***
	$\hat{f}_{14}/f_0$ (%)	**11**	***45***	***23***	*10*
	$\hat{f}_{24}/f_0$ (%)	***21***	***47***	***24***	***24***
0.5	$(f_1 - f_0)/f_0$ (%)	*3*	**8**	*6*	***18***
	$(f_2 - f_0)/f_0$ (%)	***29***	***27***	***27***	***95***
	$(f_4 - f_0)/f_0$ (%)	***−47***	***−10***	***−37***	***−23***
	$(f_5 - f_0)/f_0$ (%)	***−45***	***−76***	***−74***	***−82***
	$\hat{f}_{15}/f_0$ (%)	*3*	*12*	*11*	*2*
	$\hat{f}_{24}/f_0$ (%)	***39***	***88***	***52***	***57***
	$\hat{f}_{34}/f_0$ (%)	***15***	***33***	**11**	***32***

for runs initialized with LAPS analyses, the largest positive impact on rain rate, associated with a statistically significant decrease in areal coverage, for the lighter threshold was due to a change from KF to NC (Jankov et al. 2005). Changes in the microphysics (from MPN to both MPL and MPF) also resulted in a statistically significant increase of the rain rate but with lower levels of confidence. For the heavier threshold, only the change from MPN to MPL had a statistically significant impact (increase) on rain rate. None of the synergistic interactions between the physical schemes had a statistically significant impact on the rain rate for both thresholds.

Runs initialized with the Eta analyses behaved similarly to those initialized with the LAPS analyses for the 0.01-in. threshold, with the largest impact on rain rate being due to changes in the convective treatment from KF to both BMJ (which resulted in a large decrease of rain rate due to the BMJ scheme's tendency to overpredict areal coverage and underpredict amounts compared with the control run) and NC (which resulted in a large increase of rain rate due to the NC scheme's tendency to underpredict areal coverage compared

with the control run), and less of a positive impact due to changes in the microphysics. For the 0.5-in. threshold, the largest impact (negative) on rain rate, associated with a statistically significant increase in areal coverage (not shown), was due to a change from KF to BMJ. This might be expected as a consequence of the BMJ scheme tendency to underpredict heavier amounts. In addition, changes in the microphysics increased the rain rate (statistically significant with a lower level of confidence).

In contrast to runs initialized with the LAPS analyses, runs initialized with the Eta analyses differed in the magnitude of the synergistic interactions among the different schemes, with several having a statistically significant impact on the simulated rain rate. For the 0.01-in. threshold a synergistic interaction between MPL and NC resulted in a notable increase in rain rate with a 95% level of confidence. Specifically, both changes from MPN to MPL and from KF to NC increased the rain rate, and the synergistic interaction between MPL and NC had the same positive impact. On the other hand, changes from both MPN to MPF and from KF to NC increased the rain rate while the synergistic interaction between MPF and NC resulted in a significant (80%–90% confidence level) decrease of rain rate.

A similar trend occurred for the heavier 0.5-in. threshold for the interaction between ETA and MPF except that the confidence level was higher (95%). In addition, the interaction between MPL and NC was statistically significant, but in contrast to the 0.01-in.

threshold, the synergy contribution was positive like those of the individual changes. If the goal is not only to increase the ensemble spread by using different physical schemes but also to improve the accuracy of the simulated rainfall, information about the synergistic effect may be used as a calibration tool. Specifically, knowing how particular physical schemes and their interactions impact the simulated rainfall quantitatively may determine the choice of physical schemes used in an ensemble.

Table 3 presents the factor separation results for the rain volume. For runs initialized with LAPS analyses at both light and heavier thresholds, the largest positive impact was due to changes in the microphysics. In addition, for the 0.5-in. threshold, a change from KF to BMJ decreased the rain volume significantly. On the other hand, for runs initialized with the Eta analyses, for the 0.01-in. threshold, only a change in the PBL scheme produced a statistically significant positive impact. For the 0.5-in. threshold, both a change from KF to NC and from KF to BMJ reduced the rain volume notably. A change from MPN to MPL and from MRF to ETA resulted in an increase in the rain volume in both cases but with a lower level of statistical confidence.

In both Tables 2 and 3, the change from KF to BMJ appeared to significantly impact the simulated rainfall when 40-km Eta analyses were used, but not when LAPS analyses were used. On the other hand, a change from KF to NC had a significant impact on the simulated rainfall for both initializations. This once again may imply that the BMJ scheme used in EDAS influences the initial conditions in such a way that when a different convective scheme is used in the model, the impact on simulated rainfall is particularly large.

Finally, using Eq. (1), but with $(f_x - f_0)$ representing a change in the physical scheme and $(f_y - f_0)$ representing a change in the initial conditions, synergistic terms for both rain rate and rain volume were calculated (not shown). The synergistic term magnitudes were quite small for all physics variations for both thresholds and at all times. In addition, the majority of the synergistic terms were negative. The only exceptions were in the case of rain rate, when the change from the LAPS analyses to the Eta analyses was combined with changes from KF to both BMJ (for both thresholds) and to NC (only for the lighter threshold). Due to their small magnitudes, these data were not tested for statistical significance.

2) ILLUSTRATIVE RESULTS

Results previously presented indicated a larger sensitivity to changes in the microphysics for runs initial-

ized with the LAPS analyses compared with those initialized with the Eta analyses. This might be explained by the fact that the 40-km Eta analysis is generated by the EDAS that uses the BMJ convective scheme, which has a tendency to generate large areas of light rainfall while substantially drying the atmosphere and reducing the grid-resolved component of precipitation (e.g., Gallus 1999). Thus, runs initialized with 40-km Eta analyses may be too dry initially for microphysical schemes to activate in areas where precipitation is likely to be observed, and the role of the microphysics is restricted until later forecast times when the influence of the initial conditions has diminished. Support for this argument is provided in Fig. 5, which shows the total and grid-resolved rainfall components for the first forecast hour on 13 June 2002 for the BMJ–ETA–MPF (the NCEP operational Eta Model physical schemes) model run initialized with both the Eta and LAPS analyses. The total rainfall field from the run initialized with the Eta analysis (Fig. 5a) was characterized by a much lighter and broader rainfall area compared with the run initialized with the LAPS analysis (Fig. 5b). More importantly, Fig. 5c implies that most of the rainfall simulated during the first forecast hour by the run initialized with the Eta analysis came from the parameterized convective precipitation component. In the case of the run initialized with the LAPS analysis, a notable part of the total simulated rainfall (Fig. 5b) was resolved on the grid (Fig. 5d). Figure 6 shows the same fields as Fig. 5 but for the 17–18-h forecast period. It can be seen that later in the forecast, as the influence of the initial conditions diminished, the grid-resolved component of the rainfall for the run initialized with the Eta analysis (Fig. 6c) became more substantial, but was still smaller than it was in the run initialized with the LAPS analysis (Fig. 6d).

As an additional issue it was found that early in the forecast, for runs initialized with the LAPS analyses, the change in the PBL scheme did not notably affect the rainfall forecast, while for runs initialized with the Eta analyses, the rainfall was considerably altered. This might be related to the fact that the EDAS uses the BMJ scheme, whose structure favors activation in cases with significant amounts of moisture in low and midlevels and positive convective available potential energy (CAPE). In other words, favorable conditions for convective scheme activation associated with the Eta analyses result in an early triggering of convection, which then induces differences in the evolution of the thermodynamic profiles for runs using various PBL schemes. These differences are especially noticeable for runs initialized with the Eta analyses and they are illustrated in the following.
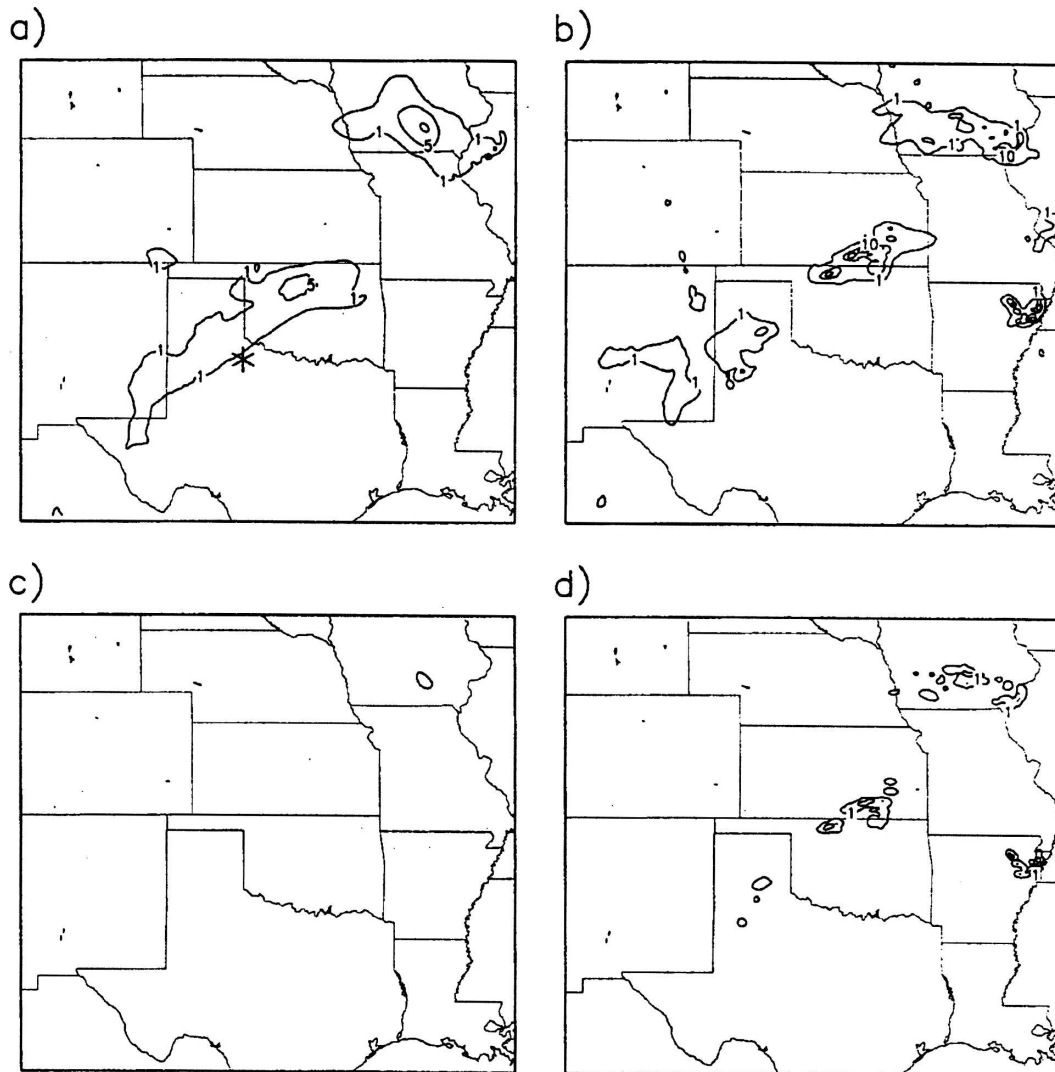
FIG. 5. Total accumulated precipitation for the 0–1-h forecast period initialized with (a) Eta and (b) LAPS. (c), (d) As in (a) and (b), respectively, but for the grid-resolved precipitation component. Based on BMJ–ETA–MPF model simulation initialized at 0000 UTC 13 Jun 2002. Contours are shown for 1, 5, 10, 20, and 30 mm.

Figure 7 presents the temporal variations of the thermodynamic profiles at the grid point (34°N, 100°W), indicated by an asterisk in Fig. 5a, for the BMJ–MRF–MPF (dashed lines) and BMJ–ETA–MPF (solid lines) model runs initialized at 0000 UTC for 13 June 2002. The two model configurations differ only in their PBL schemes (MRF versus ETA). An examination of the vertical velocity values at the location of interest indicated rather small magnitudes for both initializations. It can be seen that at this location both initializations were characterized by nearly neutral elevated mixed layers, and the Eta analysis (Fig. 7a) was slightly less stable compared with the LAPS analysis (Fig. 7b). The Eta profile was characterized by a large value of surface CAPE ($\sim$3500 J kg^{-1}) and a negligible convective in-

hibition (CIN; $\sim$1 J kg^{-1}), while in the case of the LAPS analysis, the surface CAPE was much smaller ($\sim$1300 J kg^{-1}) and the CIN was much larger ($\sim$105 J kg^{-1}). Consequently, in the run initialized with the Eta analysis the BMJ scheme activated (Fig. 7c) and produced light rainfall during the first two forecast hours. The profiles from runs that used different PBL schemes started to evolve differently. On the other hand, at this time, profiles from runs initialized with the LAPS analysis using different PBL schemes remained identical (Fig. 7d). Two hours later, in runs initialized with the Eta analysis (Fig. 7e), both profiles were characterized by a distinctive "onion" shape, but they differed notably in other ways. The profile from the run that used the MRF scheme (dashed lines) was characterized
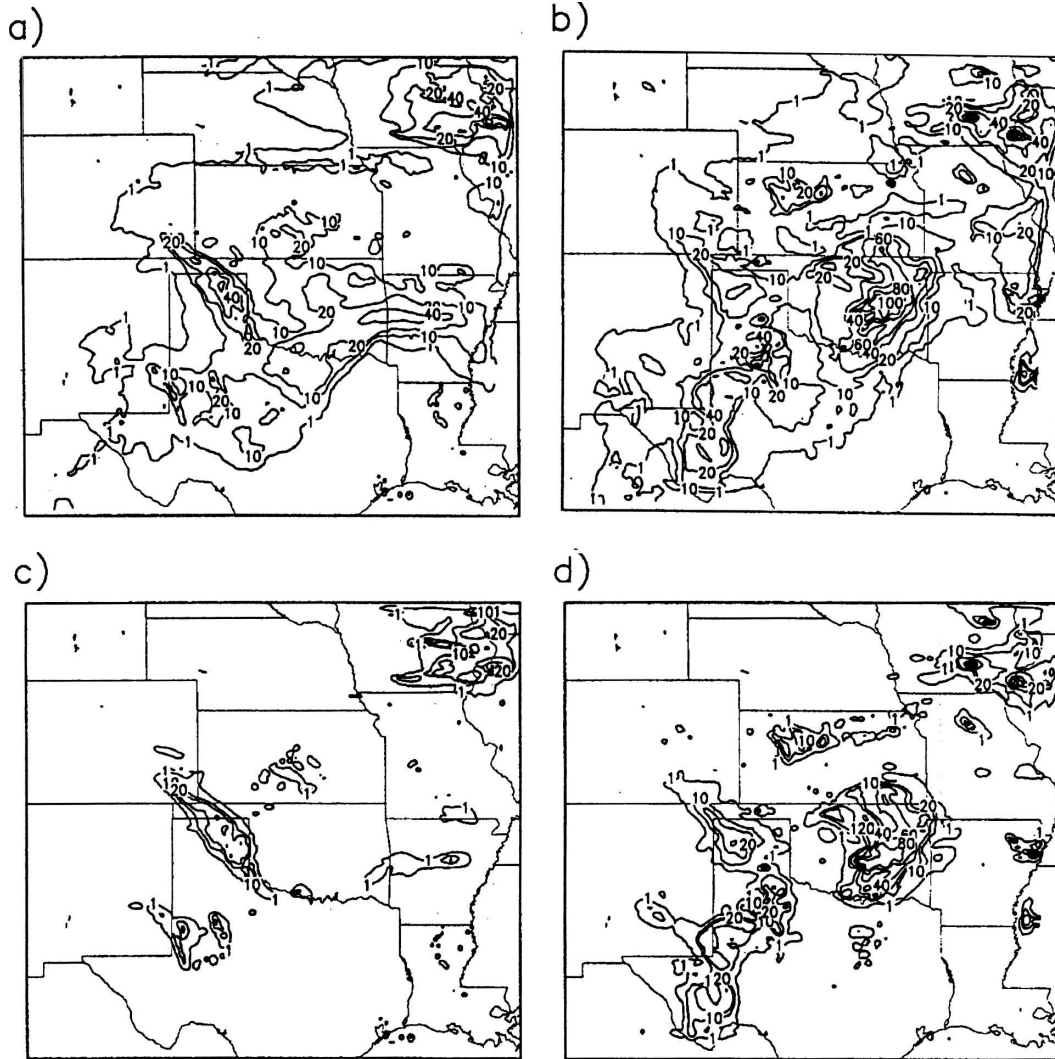
FIG. 6. As in Fig. 5 but for the 17–18-h forecast period. Contours are shown for 1, 10, and 20 mm, and then every 20 mm up to 120 mm.

by a drier and more stable boundary layer. At the same time, in runs initiated with the LAPS analysis (Fig. 7f), the convective scheme had now activated and the profiles began to differ. Even at 0600 UTC, differences between the profiles from runs that used different PBL schemes and were initialized with the Eta analysis (Fig. 7g) were larger than the difference in profiles from runs initialized with the LAPS analysis (Fig. 7h). This type of behavior among runs using different PBL schemes initialized with different initializations was frequently observed.

c. Mixed-physics and mixed initial condition ensemble skill

Results from the factor separation method indicated that for both initializations changes in the convective

treatment affected the rain rate the most. Rain volume appeared to be influenced the most by changes in the microphysics in the case of runs initialized with LAPS analyses and by changes in the convective treatment for runs initialized with the 40-km Eta analyses. This information was used in designing the four different ensembles evaluated below.

Table 4 provides the areas under relative operating characteristic (ROC) curves (Mason and Graham 1999) for an 18-member ensemble, a 9-member ensemble (including three different convective treatments, ETA PBL, and three different microphysics), and two 6-member ensembles (one including three different convective treatments, two different PBL schemes, and MPF; and another including the BMJ scheme, two different PBL schemes, and three different microphysics),
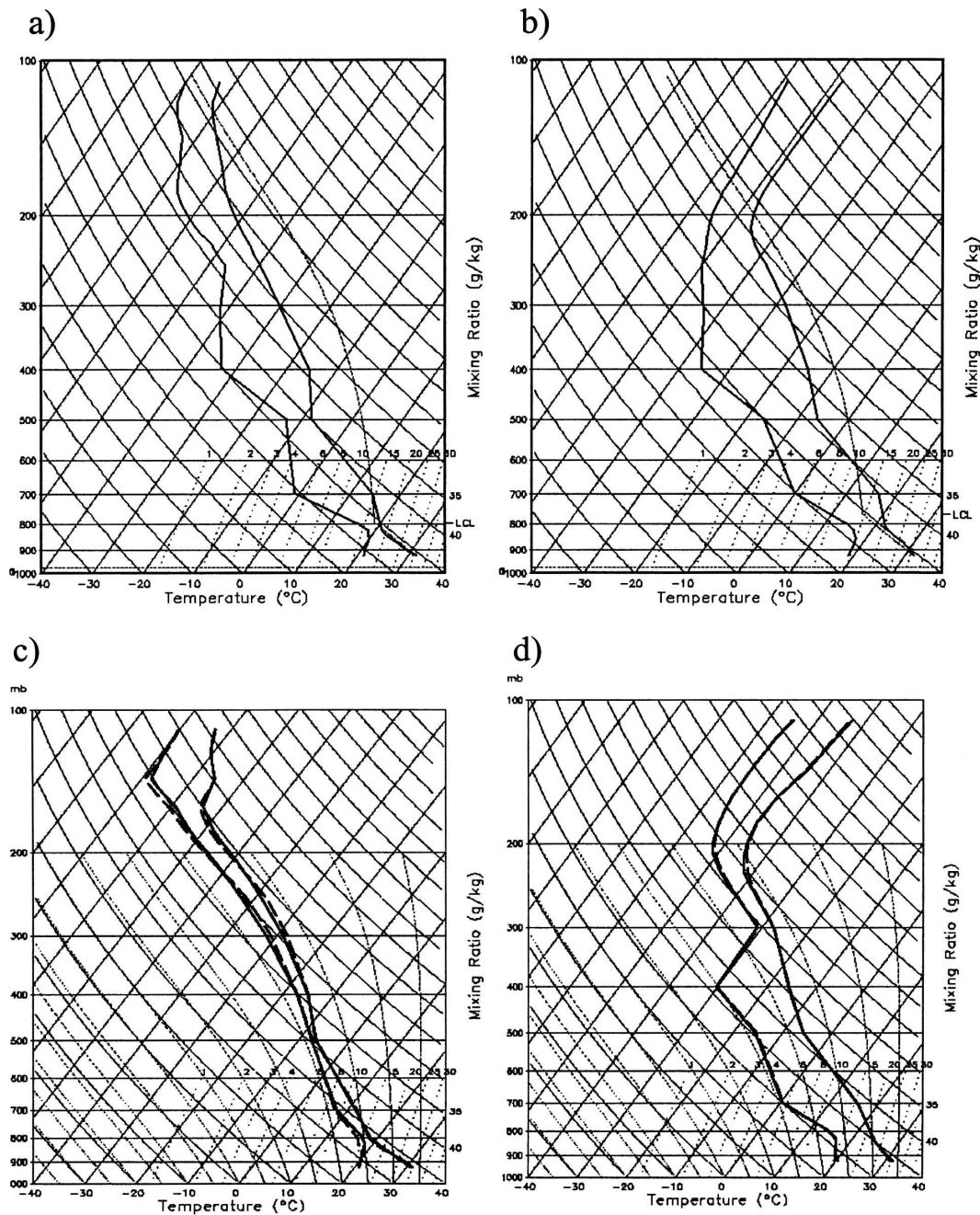
FIG. 7. The BMJ–ETA–MPF (solid lines) and BMJ–MRF–MPF (dashed lines) thermodynamic profiles from the model runs initialized with the (left) Eta and (right) LAPS analyses at the point indicated by an asterisk in Fig. 5a at (a), (b) 0000; (c), (d) 0200; (e), (f) 0400; and (g), (h) 0600 UTC.

for the 0.01- and 0.25-in. thresholds for the two different initializations during four 6-hourly forecast periods. Areas under the ROC curves are a measure of the probabilistic forecast skill of precipitation exceeding the stated threshold, with values greater than 0.5 implying the potential for a skillful forecast and values near 0.7 implying a useful forecast (Buizza et al. 1999).

It should be noted that because of differences in the bias among runs initialized with different analyses, magnitudes of areas under ROC curves for ensembles using different initial conditions should be interpreted with caution. An increase in the bias has been shown to lead to an increase in the probability of detection (Baldwin and Kain 2004) and most likely a smaller in-
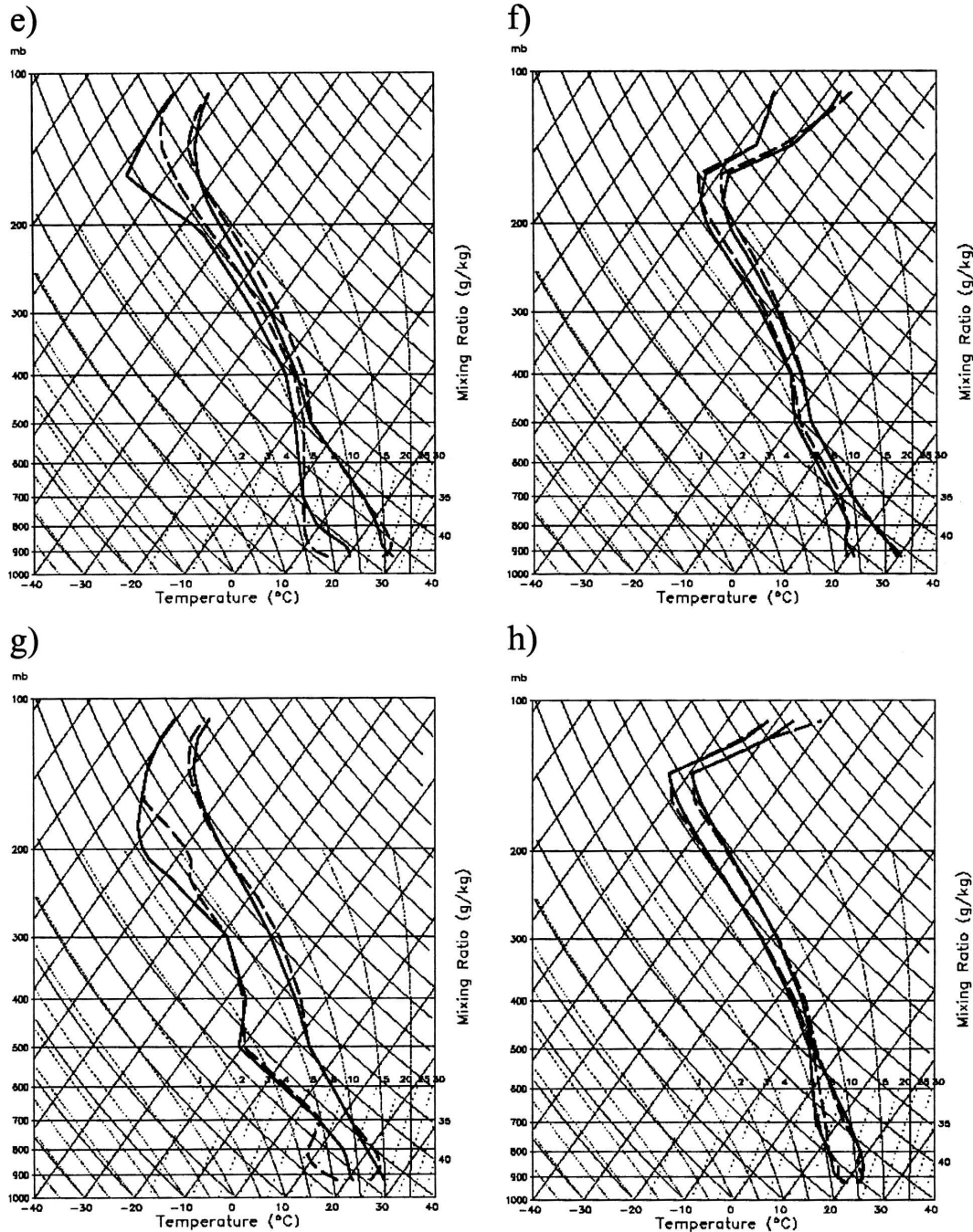
e)

f)

g)

h)

FIG. 7. (*Continued*)

crease in the probability of false detection, resulting in higher values of areas under ROC curves for ensembles with higher biases.

Because the trapezoidal approach was used for the calculation of the areas under the ROC curves, ensembles with more members would likely earn higher values (more probability thresholds exist). Despite this,

Table 4 shows larger values for the 9-member ensemble than for the 18-member one for both initializations and both thresholds. In addition, values associated with the two 6-member ensembles were generally similar to values from the full 18-member ensemble for both initializations. These results further support findings indicated by the factor separation method (identifying the

TABLE 4. Areas under ROC curves averaged for all eight cases for the 18_full ensemble (including all 18 model configurations); the nine member ensemble [9_cu_ETA_mp; including three different convective treatments (cu), ETA PBL, and three different microphysics (mp)]; and two six-member ensembles [6_cu_pbl_MPF and 6_BMJ_pbl_mp; the first including three different convective treatments and two different PBL schemes (pbl and MPF), and the second including the BMJ scheme, two different PBL schemes, and three different microphysics], for the 0.01- and 0.2-in. thresholds, for the two different initializations, and for the four specified 6-hourly forecast periods.

Threshold (in.)	Ensemble type	Area under ROC curve			
		0–6 h	6–12 h	12–18 h	18–24 h
	Runs initialized with Eta analysis				
0.01	18_full	0.802	0.721	0.691	0.720
	9_cu_ETA_mp	0.805	0.752	0.708	0.712
	6_cu_pbl_MPF	0.791	0.731	0.682	0.684
	6_BMJ_pbl_mp	0.775	0.685	0.700	0.662
0.25	18_full	0.662	0.596	0.600	0.706
	9_cu_ETA_mp	0.674	0.643	0.641	0.704
	6_cu_pbl_MPF	0.652	0.606	0.607	0.661
	6_BMJ_pbl_mp	0.640	0.546	0.590	0.624
	Runs initialized with LAPS analysis				
0.01	18_full	0.871	0.743	0.649	0.634
	9_cu_ETA_mp	0.882	0.835	0.743	0.719
	6_cu_pbl_MPF	0.851	0.797	0.711	0.703
	6_BMJ_pbl_mp	0.862	0.802	0.703	0.701
0.25	18_full	0.664	0.635	0.582	0.582
	9_cu_ETA_mp	0.674	0.694	0.619	0.602
	6_cu_pbl_MPF	0.644	0.638	0.591	0.600
	6_BMJ_pbl_mp	0.637	0.605	0.552	0.558

convective and microphysical treatments as those affecting simulated MCS rainfall the most) in the design of the ensembles.

Areas under ROC curves were also computed for ensembles that combined various physical schemes and different initial conditions (not shown). It was found that runs initialized with Eta analyses using different convective treatments combined with runs initialized with LAPS analyses using various microphysics tended to have the largest scores, but the scores were lower than scores from ensembles initialized with the LAPS analyses presented in Table 4. This might be explained by the bias differences among the ensemble members.

In addition, rank histograms (see, e.g., Hamill 2001) were created based on the gridded precipitation forecast by each member of the ensembles listed in Table 4 and for both initial conditions. Because histograms related to different initial conditions showed the same general trend, only those associated with the Eta initial conditions will be presented. Figure 8 shows these for the 0–6-h forecast periods, and Fig. 9 for the 12–18-h forecast periods. During the 0–6-h forecast period, the histogram for the full 18-member ensemble (Fig. 8a)
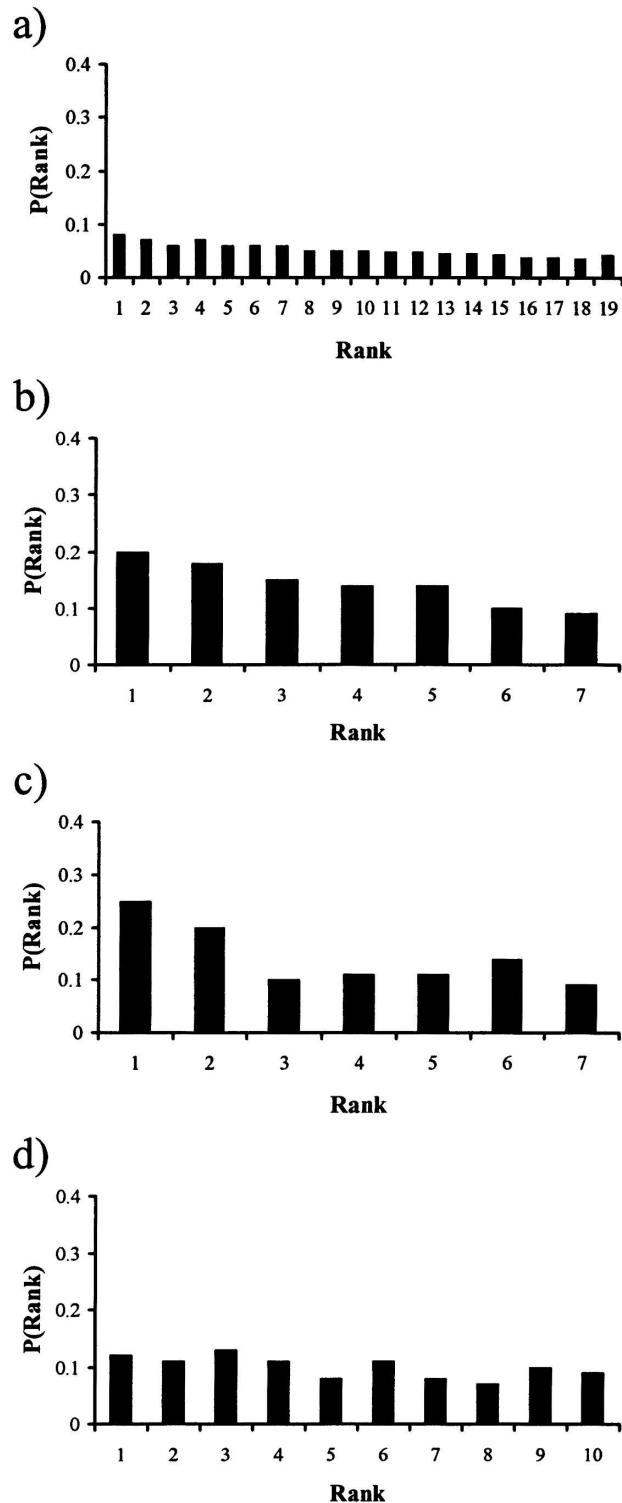
FIG. 8. Rank histograms for the (a) 18_full, (b) 6_cu_pbl_MPF, (c) 6_BMJ_pbl_mp, and (d) 9_cu_ETA_mp ensembles (see Table 4 caption for the notation legends), for the 0–6-h forecast period and using the Eta initial conditions.
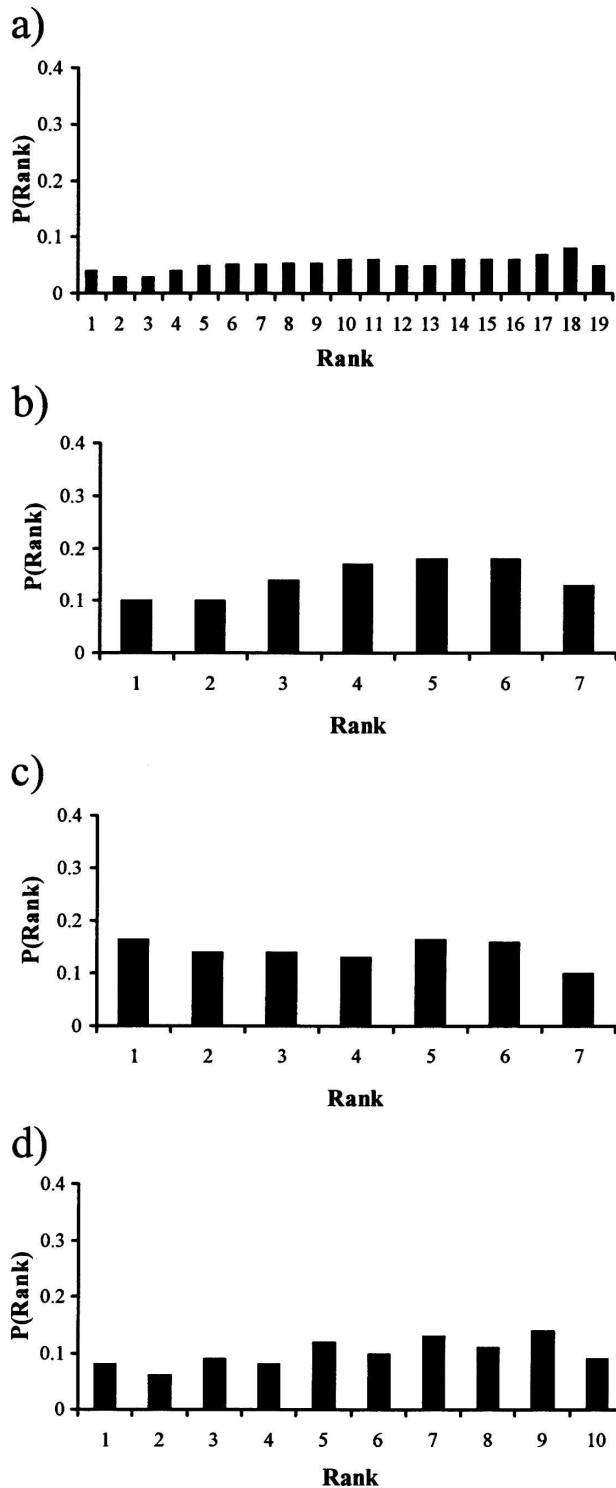
a)

b)

c)

d)

FIG. 9. As in Fig. 8 but for the 12–18-h forecast period.

indicates that the ensemble members were too wet compared with the observations. The same trend was present in histograms related to the two six-member ensembles (Figs. 8b and 8c), especially in the case of the

ensemble using the BMJ scheme (Fig. 8c). More precisely, this trend was present for all ensembles involving different convective treatments combined with different PBL schemes except when NC runs were the only ones used. When only NC runs were used, the rank histogram had a U shape, indicating insufficient spread (not shown). Additionally, ranked histograms were created using physical schemes from the two six-member ensembles but combining different initial conditions (not shown). The tendency of the ensemble members to be too wet was reduced, although it was still present. This may imply that the use of a combination of diabatic hot-start and cold-start initial conditions in an ensemble designed for rainfall forecast might reduce the bias related to light rainfall at earlier times. On the other hand, the histogram for the nine-member ensemble, which combined different convective treatments and different microphysical schemes (Fig. 8d), showed reasonable spread.

For the 12–18-h forecast period, histograms related to the full 18-member ensemble (Fig. 9a) suggest a slight underforecasting of precipitation during the 12–18-h forecast period, while a 6-member ensemble using BMJ (Fig. 9c), and a 9-member ensemble, (Fig. 9d) indicate a generally reasonable spread. On the other hand, the histogram shape for the six-member ensemble, which included three different convective treatments, two different PBL schemes, and MPF, indicates a slight overdispersion.

4. Summary and discussion

General trends in the impact of various physical schemes and their interactions on warm season, continental MCS rainfall forecasts were evaluated under different initial conditions. A matrix of 18 WRF–ARW model configurations with 12-km grid spacing was created using different physical scheme combinations for eight IHOP MCS cases. For each case, three different treatments of convection were used, with three different microphysical schemes and two different PBL schemes. The runs were initialized with both a diabatic LAPS hot start initialization (Jian et al. 2003) and 40-km Eta GRIB files.

ETS and bias analyses of the 288 WRF–ARW model simulations considered in the present study indicated that for both initializations no single model configuration was clearly best for the entire simulation period and for all thresholds. Differences in ETS and bias for runs initialized with different initial conditions but using the same model configuration, as well as ETS and bias changes for runs initialized with the two different

initial conditions but with changes in the model configuration, were often statistically significant, implying that both variations in the physics and the initial conditions may be applied to increase the spread of an ensemble used for MCS rainfall forecasting.

The factor separation method (Stein and Alpert 1993) was used to quantify the impacts of the variation of two different physical schemes compared with a control run (KF–MRF–MPN) and their interaction (synergy) on the simulated rainfall. For both initializations, changes in convective treatment affected the rain rate the most. For runs initialized with the LAPS analyses, rain volume was affected the most by changes in the microphysics, while for runs initialized with the 40-km Eta analyses, the rain volume was influenced most by the choice of the convective treatment. Information about the interactions among different physical schemes obtained through the synergistic term analysis should be useful in an ensemble calibration procedure.

Rank histograms and areas under ROC curves were examined for ensembles using these various model configurations and different initial conditions. Findings supported the results from the factor separation methodology, which identified convective and microphysical treatments as those with the largest impact on the simulated MCS rainfall.

In conclusion, it appears that the sensitivity of the WRF–ARW model rainfall forecasts to the use of varied physical schemes and their interactions is dependent on the initialization dataset or procedure. If an ensemble designed for MCS rainfall prediction lacks sufficient spread, model runs with different convective schemes should be included. If rain volume is a desired quantity (e.g., hydrological purposes), and an initialization uses the LAPS analyses, runs with the MPL and MPF microphysical schemes may require different bias corrections or weightings in an ensemble compared to runs using MPN. In contrast, when the Eta analysis is used for initialization, runs with these different microphysical schemes may not need such different weightings, but runs with NC and BMJ would require different weightings as compared to KF runs. Knowledge of which physical schemes exert the greatest impact on rainfall forecasts can allow for the design of ensembles that maximize skill while minimizing the number of members needed.

TABLE A1. Time series of percentage changes in system rain rate and domain rain volume, averaged for two cases (0000 UTC 4 Jun and 0000 UTC 13 Jun), because of the code fix for runs using different convective treatment (KF and NC) averaged over points where rainfall exceeded specified thresholds (0.01 and 0.5 in.).

Threshold (in.)	Forecast period (h)			
	00–06	06–12	12–18	18–24
	NC reruns			
	System-average rain rate			
0.01	−20%	3%	−7%	−7%
0.5	0%	4%	−11%	−6%
	Domain-total rain volume			
0.01	22%	0%	−20%	19%
0.5	23%	0%	−21%	−12%
	KF reruns			
	System-average rain rate			
0.01	21%	−8%	4%	11%
0.5	17%	8%	4%	10%
	Domain-total rain volume			
0.01	24%	19%	18%	23%
0.5	22%	19%	15%	21%

APPENDIX A

Sensitivity of System-Average Rain Rate and Domain-Total Rain Volume to "Bug" in Radiation Code

Late in the review process it came to the authors' attention that in the official, publicly distributed version of the WRF model code a bug related to the MPF scheme had been found (this had affected all versions of the model through that point in time). For the WRF configurations using MPF, the short- and longwave radiation codes did not consider the four condensates available from MPF (cloud water, cloud ice, rain, and "precipitating" ice). Instead, the radiative codes used only the total amount of the four condensates from MPF, treating this total condensate as cloud ice or water depending on the temperature (with 273.15 K as a threshold point). In this way an artificial microphysics dependency on radiation was introduced, distinct from that due to the difference in the mixing ratio of the various species produced by MPF itself. Effectively, a less refined cloud–radiation interaction than intended was used for simulations with the MPF configuration. Practically, it was not feasible to rerun the entire relevant simulations with a code fix when the code bug issue was pointed out. Additionally, the same code was used also in Jankov et al. (2005) whose results are used extensively for comparison purposes in the present study.

Given the above, a selective series of tests was per-

TABLE B1. ETS and bias (in parentheses) values averaged over the eight IHOP cases for different physical-scheme combinations for the 0–6-h forecast period for four different rainfall thresholds and for two different initializations. The notation presented in Table 1 is used to indicate different model configurations. The maximum values are indicated in boldface.

Run	Threshold (in.)			
	0.01	0.10	0.50	1.0
KF–MRF–MPN–Eta	0.220 (1.6)	0.165 (1.8)	0.095 (2.2)	**0.052** (2.7)
KF–MRF–MPN–LAPS	0.265 (1.6)	0.211 (1.8)	0.067 (1.1)	0.041 (0.4)
KF–ETA–MPL–Eta	0.207 (2.1)	0.154 (2.3)	0.081 (2.7)	0.040 (3.8)
KF–ETA–MPL–LAPS	0.235 (2.4)	0.187 (2.6)	0.077 (1.8)	0.055 (0.8)
KF–ETA–MPN–Eta	0.209 (1.9)	0.156 (2.0)	0.086 (2.2)	0.045 (2.7)
KF–ETA–MPN–LAPS	0.242 (2.0)	0.201 (2.1)	0.066 (1.2)	0.033 (0.4)
KF–ETA–MPF–Eta	0.216 (1.9)	0.156 (2.2)	0.085 (2.5)	0.039 (3.3)
KF–ETA–MPF–LAPS	0.272 (1.8)	0.205 (2.1)	0.090 (2.2)	**0.063** (1.2)
KF–MRF–MPL–Eta	0.227 (1.9)	0.165 (2.1)	0.085 (2.7)	0.044 (3.7)
KF–MRF–MPL–LAPS	0.255 (2.1)	0.196 (2.6)	0.073 (1.8)	0.059 (1.2)
KF–MRF–MPF–Eta	0.225 (1.8)	0.164 (2.1)	0.083 (2.6)	0.049 (3.2)
KF–MRF–MPF–LAPS	0.276 (1.8)	0.206 (2.1)	0.075 (1.4)	0.038 (0.5)
NC–ETA–MPL–Eta	**0.233** (0.9)	0.167 (1.1)	0.064 (2.3)	0.035 (4.8)
NC–ETA–MPL–LAPS	**0.349** (1.0)	**0.247** (1.3)	0.086 (1.9)	0.044 (1.2)
NC–ETA–MPN–Eta	0.211 (0.7)	0.161 (0.8)	0.051 (1.2)	0.027 (2.4)
NC–ETA–MPN–LAPS	0.327 (0.8)	0.215 (1.8)	0.048 (0.9)	0.022 (0.5)
NC–ETA–MPF–Eta	0.224 (0.9)	0.169 (1.1)	0.081 (1.8)	0.044 (2.8)
NC–ETA–MPF–LAPS	0.298 (1.1)	0.203 (1.4)	0.055 (0.8)	0.041 (0.5)
NC–MRF–MPL–Eta	**0.236** (0.8)	0.161 (0.9)	0.058 (1.8)	0.035 (3.6)
NC–MRF–MPL–LAPS	0.308 (1.1)	0.201 (1.5)	0.066 (1.0)	0.039 (0.8)
NC–MRF–MPN–Eta	0.200 (0.5)	0.142 (0.5)	0.034 (0.8)	0.017 (1.6)
NC–MRF–MPN–LAPS	0.304 (0.7)	0.191 (0.7)	0.057 (0.3)	0.029 (0.4)
NC–MRF–MPF–Eta	**0.258** (0.9)	**0.181** (1.1)	0.085 (1.7)	0.048 (2.6)
NC–MRF–MPF–LAPS	0.311 (1.1)	0.208 (1.4)	0.057 (1.0)	0.032 (1.0)
BMJ–ETA–MPL–Eta	0.223 (2.2)	**0.185 (2.4)**	0.096 (1.9)	0.034 (2.4)
BMJ–ETA–MPL–LAPS	0.246 (2.1)	0.167 (2.6)	**0.100 (1.0)**	0.053 (0.6)
BMJ–ETA–MPN–Eta	0.217 (2.1)	**0.180 (2.2)**	**0.107 (1.5)**	0.017 (1.5)
BMJ–ETA–MPN–LAPS	0.249 (2.2)	0.182 (2.6)	0.070 (0.8)	0.026 (0.5)
BMJ–ETA–MPF–Eta	**0.254** (2.0)	**0.215 (1.9)**	**0.152 (0.9)**	0.042 (0.6)
BMJ–ETA–MPF–LAPS	0.249 (2.4)	0.177 (2.8)	0.079 (1.1)	0.029 (0.8)
BMJ–MRF–MPL–Eta	0.225 (2.3)	**0.180 (2.4)**	**0.094 (1.9)**	0.037 (2.3)
BMJ–MRF–MPL–LAPS	0.249 (2.4)	0.179 (2.8)	0.099 (0.7)	0.054 (0.5)
BMJ–MRF–MPN–Eta	0.219 (2.1)	**0.175 (2.2)**	**0.104 (1.5)**	0.021 (1.1)
BMJ–MRF–MPN–LAPS	0.249 (2.1)	0.178 (2.5)	**0.100 (0.7)**	0.046 (0.3)
BMJ–MRF–MPF–Eta	0.223 (2.2)	**0.187 (2.2)**	**0.095 (1.7)**	0.035 (2.2)
BMJ–MRF–MPF–LAPS	0.252 (2.5)	0.180 (2.7)	0.074 (1.0)	0.038 (0.4)

formed in order to evaluate the relative impact that the code fix may have. In the evaluation two randomly selected cases from the present study, both initialized with Eta analyses at 0000 UTC, were used. Simulations of these two cases with and without the code fix were performed by using the latest version (2.1.2) of the WRF model and two different convective treatments (NC and KF). All reruns used MRF and MPF. For these runs system-average rain rates and domain-total rain volumes were recalculated. Relative changes in these two measures between runs with and without the code fix are presented in Table A1. The results indicate that the code fix mainly affected the domain-total rain volume, especially for runs using KF. Also, in the case of the KF runs the code fix generally caused an increase in both system-average rain rate and domain-total rain volume, while in the case of the NC runs, decreases were indicated occasionally. Based on the tendencies in the original results and the general trend of the difference between runs with and without the code fix, it can be suggested that the code fix should not affect the general conclusions (i.e., for the 0.01-in. threshold, a change in rain rate due to the fix in MPF will be more pronounced; the opposite will be the case for the 0.5-in. threshold; with regard to rain volume, for both thresholds the large increase would be even more pronounced when the version of the model with the MPF code fixed is used). In addition, ETS and bias values were calculated for the two configurations and averaged over the two cases. The code fix generated only small differ-

TABLE B2. As in Table B1 but for the 12–18-h period.

Run	Threshold (in.)			
	0.01	0.10	0.50	1.0
KF–MRF–MPN–Eta	0.138 (1.2)	0.115 (1.3)	**0.100** (1.3)	0.015 (1.9)
KF–MRF–MPN–LAPS	0.169 (1.3)	0.155 (1.7)	0.091 (1.0)	0.027 (0.8)
KF–ETA–MPL–Eta	0.134 (2.1)	0.100 (2.3)	0.086 (1.9)	0.027 (2.4)
KF–ETA–MPL–LAPS	0.160 (2.1)	0.145 (1.9)	0.102 (1.4)	0.029 (1.4)
KF–ETA–MPN–Eta	0.146 (1.7)	0.129 (1.7)	0.085 (1.5)	0.022 (1.8)
KF–ETA–MPN–LAPS	0.168 (1.8)	0.157 (1.6)	0.089 (1.3)	0.018 (0.9)
KF–ETA–MPF–Eta	0.117 (1.8)	0.100 (2.0)	0.068 (1.6)	0.009 (1.8)
KF–ETA–MPF–LAPS	0.133 (2.0)	0.122 (1.8)	0.105 (1.0)	0.027 (1.0)
KF–MRF–MPL–Eta	0.148 (1.5)	0.111 (1.7)	0.089 (1.7)	0.017 (2.3)
KF–MRF–MPL–LAPS	0.177 (1.7)	0.146 (1.7)	0.103 (2.5)	**0.047** (1.6)
KF–MRF–MPF–Eta	0.130 (1.4)	0.104 (1.6)	0.089 (1.4)	0.018 (1.6)
KF–MRF–MPF–LAPS	0.172 (1.5)	0.141 (1.5)	0.085 (2.6)	0.023 (1.3)
NC–ETA–MPL–Eta	0.154 (1.0)	0.098 (1.1)	0.061 (1.6)	0.015 (3.1)
NC–ETA–MPL–LAPS	0.156 (1.4)	0.152 (1.0)	0.079 (1.9)	0.016 (1.4)
NC–ETA–MPN–Eta	0.164 (1.0)	0.121 (0.9)	**0.101** (1.1)	**0.045** (2.2)
NC–ETA–MPN–LAPS	0.156 (1.3)	0.152 (1.0)	0.079 (0.9)	0.016 (1.1)
NC–ETA–MPF–Eta	0.137 (1.1)	0.092 (1.2)	0.052 (1.5)	0.034 (2.0)
NC–ETA–MPF–LAPS	0.164 (1.4)	0.151 (1.1)	0.057 (2.3)	0.014 (1.5)
NC–MRF–MPL–Eta	0.148 (0.6)	0.110 (0.7)	0.083 (1.2)	0.026 (2.6)
NC–MRF–MPL–LAPS	**0.239 (1.1)**	**0.213 (1.0)**	0.113 (1.5)	0.043 (1.4)
NC–MRF–MPN–Eta	0.107 (0.6)	0.070 (0.6)	0.067 (0.8)	0.037 (1.3)
NC–MRF–MPN–LAPS	0.211 (0.8)	0.195 (0.8)	**0.118 (0.7)**	0.040 (0.5)
NC–MRF–MPF–Eta	0.145 (0.8)	0.111 (0.9)	**0.092** (1.1)	**0.062** (1.6)
NC–MRF–MPF–LAPS	0.181 (1.1)	0.159 (1.2)	0.077 (1.1)	0.034 (0.9)
BMJ–ETA–MPL–Eta	**0.169 (2.0)**	**0.150 (2.1)**	0.041 (0.8)	0.005 (0.5)
BMJ–ETA–MPL–LAPS	0.167 (2.1)	0.141 (2.8)	0.064 (1.4)	0.020 (0.5)
BMJ–ETA–MPN–Eta	**0.187 (1.9)**	**0.166 (1.9)**	0.038 (0.6)	0.000 (0.2)
BMJ–ETA–MPN–LAPS	0.162 (2.2)	0.148 (2.7)	0.065 (1.2)	0.014 (0.4)
BMJ–ETA–MPF–Eta	**0.202 (2.0)**	**0.164 (2.1)**	0.026 (0.9)	0.001 (0.6)
BMJ–ETA–MPF–LAPS	0.160 (2.1)	0.145 (2.6)	0.053 (1.0)	0.020 (0.3)
BMJ–MRF–MPL–Eta	**0.172 (1.9)**	**0.149 (2.1)**	0.041 (0.6)	0.001 (0.3)
BMJ–MRF–MPL–LAPS	0.176 (2.0)	0.148 (1.6)	0.065 (1.4)	0.022 (0.6)
BMJ–MRF–MPN–Eta	**0.190 (1.7)**	**0.164 (1.8)**	0.037 (0.6)	0.006 (0.1)
BMJ–MRF–MPN–LAPS	0.168 (1.8)	0.145 (1.5)	0.043 (1.4)	0.009 (0.2)
BMJ–MRF–MPF–Eta	0.159 (1.9)	**0.125 (1.9)**	0.050 (0.7)	0.000 (0.4)
BMJ–MRF–MPF–LAPS	0.160 (2.0)	0.126 (1.5)	0.061 (1.6)	0.015 (0.5)

ences in the ETS and bias (up to about 5%), and infrequently resulted in a slight improvement of their values (not shown).

Finally, in the present study 288 simulations were carried out, and only 1/6 contained the MPF scheme. With this weighting for the MPF scheme, although some uncertainties are present in the MPF results due to the presence of the radiation bug, the general conclusions reached in this study are not likely to be affected.

APPENDIX B

ETS and Bias Values for 8 Cases and 18 Model Configurations

ETSs and bias values averaged for all eight cases for all 18 model configurations, for the 0–6- (Table B1) and

12–18-h (Table B2) forecast periods, computed for four different thresholds (0.01, 0.1, 0.5, and 1.00 in.) and for both initializations, indicate generally lower scores at later times. Scores are always higher for lighter than heavier thresholds. For the 0–6-h forecast period for the 0.01-in. threshold, the ETS is always higher for KF runs initialized with LAPS analyses than for ones using Eta input. Also, for the heavier threshold these runs are characterized with lower bias values. On the other hand, for KF runs initialized with Eta analyses the bias increases with threshold for all combinations of the other physics, while the opposite is the case when the LAPS analyses are used.

For the 12–18-h forecast period for the 0.01-in. threshold, the BMJ runs initialized with the Eta analyses are almost always characterized with higher ETSs compared to runs initialized with the LAPS analyses.

At the same time the BMJ runs have higher bias values than do the KF or NC runs, with the lowest bias associated with NC runs. For almost all BMJ entries in the table, the bias notably decreases with an increasing threshold.

In conclusion, ETS and bias analyses indicated that no one configuration was obviously best at all times for all thresholds with both initializations.

REFERENCES

Baldwin, M. E., and K. E. Mitchell, 1997: The NCEP hourly multi-sensor U.S. precipitation analysis for operations and GCIP research. Preprints, *13th Conf. on Hydrology,* Long Beach, CA, Amer. Meteor. Soc., 54–55.

——, and J. S. Kain, 2004: Examining the sensitivity of various performance measures. Preprints, *17th Conf. on Probability and Statistics in the Atmospheric Sciences,* Seattle, WA, Amer. Meteor. Soc., CD-ROM, 2.9.

Betts, A. K., 1986: A new convective adjustment scheme. Part I: Observational and theoretical basis. *Quart. J. Roy. Meteor. Soc.,* **112,** 677–692.

——, and M. J. Miller, 1986: A new convective adjustment scheme. Part II: Single column tests using GATE wave, BOMEX, ATEX and arctic air-mass data sets. *Quart. J. Roy. Meteor. Soc.,* **112,** 693–709.

Buizza, R., A. Hollingsworth, F. Lalaurette, and A. Ghelli, 1999: Probabilistic predictions of precipitation using the ECMWF Ensemble Prediction System. *Wea. Forecasting,* **14,** 168–189.

Chen, F., and J. Dudhia, 2001: Coupling an advanced land surface–hydrology model with the Penn State–NCAR MM5 modeling system. Part I: Model implementation and sensitivity. *Mon. Wea. Rev.,* **129,** 569–585.

Dudhia, J., 1989: Numerical study of convection observed during the Winter Monsoon Experiment using a mesoscale two-dimensional model. *J. Atmos. Sci.,* **46,** 3077–3107.

Ferrier, B. S., Y. Jin, Y. Lin, T. Black, E. Rogers, and G. DiMego, 2002: Implementation of a new grid-scale cloud and rainfall scheme in the NCEP Eta model. Preprints, *15th Conf. on Numerical Weather Prediction,* San Antonio, TX, Amer. Meteor. Soc., 280–283.

Gallus, W. A., Jr., 1999: Eta simulations of three extreme rainfall events: Impact of resolution and choice of convective scheme. *Wea. Forecasting,* **14,** 405–426.

Grimit, E. P., and C. F. Mass, 2002: Initial results of a mesoscale short-range ensemble forecasting system over the Pacific Northwest. *Wea. Forecasting,* **17,** 192–205.

Hamill, T. M., 1999: Hypothesis test for evaluating numerical precipitation forecasts. *Wea. Forecasting,* **14,** 155–167.

——, 2001: Interpretation of rank histograms for verifying ensemble forecasts. *Mon. Wea. Rev.,* **129,** 550–560.

Hong, S.-Y., and H.-L. Pan, 1996: Nonlocal boundary layer vertical diffusion in a medium-range forecast model. *Mon. Wea. Rev.,* **124,** 2322–2339.

——, H.-M. H. Juang, and Q. Zhao, 1998: Implementation of prognostic cloud scheme for a regional spectral model. *Mon. Wea. Rev.,* **126,** 2621–2639.

Janjić, Z., 1994: The step-mountain Eta coordinate model: Further developments of the convection closure schemes. *Mon. Wea. Rev.,* **122,** 927–945.

——, 2001: Nonsingular implementation of the Mellor–Yamada level 2.5 scheme in the NCEP Meso Model. NCEP Office Note 437, 61 pp. [Available online at www.emc.ncep. noaa.gov/officenotes/newernotes/on437.pdf.]

Jankov, I., and W. A. Gallus Jr., 2004: Contrast between good and bad forecasts of warm season MCS rainfall. *J. Hydrol.,* **288,** 122–152.

——, ——, M. Segal, B. Shaw, and S. E. Koch, 2005: The impact of different WRF model physical parameterizations and their interactions on warm season MCS rainfall. *Wea. Forecasting,* **20,** 1048–1060.

Jian, G.-J., S.-L. Shieh, and J. A. McGinley, 2003: Precipitation simulation associated with Typhoon Sinlaku (2002) in Taiwan area using the LAPS diabatic initialization for MM5. *Terr. Atmos. Oceanic Sci.,* **14,** 261–288.

Kain, J. S., 2004: The Kain–Fritsch convective parameterization: An update. *J. Appl. Meteor.,* **43,** 170–181.

——, and J. M. Fritsch, 1993: The role of the convective "trigger function" in numerical prediction of mesoscale convective systems. *Meteor. Atmos. Phys.,* **49,** 93–106.

Lin, Y.-L., R. D. Farley, and H. D. Orville, 1983: Bulk scheme of the snow field in a cloud model. *J. Climate Appl. Meteor.,* **22,** 1065–1092.

Mason, I., 1989: Dependence of the critical success index on sample climate and threshold probability. *Aust. Meteor. Mag.,* **37,** 75–81.

Mason, S. J., and N. E. Graham, 1999: Conditional probabilities, relative operating characteristics, and relative operating levels. *Wea. Forecasting,* **14,** 713–725.

Mlawer, E. J., S. J. Taubman, P. D. Brown, M. J. Iacono, and S. A. Clough, 1997: Radiative transfer for inhomogeneous atmospheres: RRTM, a validated correlated-k model for the longwave. *J. Geophys. Res.,* **102D,** 16 663–16 682.

Schaefer, J. T., 1990: The critical success index as an indicator of warning skill. *Wea. Forecasting,* **5,** 570–575.

Stein, U., and P. Alpert, 1993: Factor separation in numerical simulations. *J. Atmos. Sci.,* **50,** 2107–2115.

Stensrud, D. J., J.-W. Bao, and T. T. Warner, 2000: Using initial condition and model physics perturbations in short-range ensemble simulations of mesoscale convective systems. *Mon. Wea. Rev.,* **128,** 2077–2107.

Troen, I., and L. Mahrt, 1986: A simple model of the atmospheric boundary layer: Sensitivity to surface evaporation. *Bound.-Layer Meteor.,* **47,** 129–148.

Weckwerth, T. M., and D. B. Parsons, 2006: A review of convection initiation and motivation for IHOP_2002. *Mon. Wea. Rev.,* **134,** 5–22.